

ORDERING OF PARTICULATE SUSPENSIONS IN COUETTE FLOW
AT MODERATE REYNOLDS NUMBERS

By

MARTIN DEREK BELL

B.Sc., Bristol University, U.K., 1986

A THESIS SUBMITTED IN PARTIAL FULFILLMENT OF
THE REQUIREMENTS FOR THE DEGREE OF
MASTER OF SCIENCE

in

THE FACULTY OF GRADUATE STUDIES

(Department of Chemistry)

We accept this thesis as conforming
to the required standard

THE UNIVERSITY OF BRITISH COLUMBIA

August 1990

© Martin Derek Bell, 1990

In presenting this thesis in partial fulfilment of the requirements for an advanced degree at the University of British Columbia, I agree that the Library shall make it freely available for reference and study. I further agree that permission for extensive copying of this thesis for scholarly purposes may be granted by the head of my department or by his or her representatives. It is understood that copying or publication of this thesis for financial gain shall not be allowed without my written permission.

Department of CHEMISTRY

The University of British Columbia
Vancouver, Canada

Date 12/10/1990.

Abstract

A remarkable ordering phenomenon has been seen to occur when a suspension of particles undergoes shear at particle Reynolds numbers of the order of or greater than one in the annular gap of a Couette type shearing device. This particulate ordering was observed and studied with both suspensions of rigid spheres and suspensions of polystyrene latex aggregates formed in the presence of shear within the gap. Each of these systems was studied under a variety of initial conditions in order to define the particular flow conditions required for particle alignment to occur. It was found that particulate ordering occurred under similar conditions to those used by Segré and Silberberg (35) to observe the "necklace formations" that formed within particulate suspensions flowing inside tubes. The separations between aligned particles was found to be strongly dependent on the particle Reynolds number and the ratio between the particle diameter and the width of the annular gap. An insight into the hydrodynamic interactions occurring was provided by the comparisons made between the ordered aggregates and the ordered rigid spheres under similar flow conditions.

Table of Contents

<u>Abstract</u>	i
<u>Table of Contents</u>	ii
<u>List of Tables</u>	iv
<u>List of Figures</u>	vi
<u>Acknowledgements</u>	vii
<u>Chapter One. Introduction</u>	1
<u>Chapter Two. Experimental Methods</u>	13
2.1 Preparation Of Latex And Solid Bead Suspensions.....	13
2.2 Experimental Apparatus And Arrangement.....	15
2.3 Image Analysis.....	19
<u>Chapter Three. Results And Discussion</u>	22
3.1 a Introduction To Dimensionless Parameters.....	22
3.1 b Error Analysis.....	24
<u>3.2 Salt Aggregated Latex</u>	24
3.2 a Effects Of Altering The Shear Rate.....	28
3.2 b Effects Of Changing The Latex Concentration.....	32
3.2 c Effects Of Altering The Salt Concentration.....	35
<u>3.3 Rigid Monodisperse Polymer Spheres</u>	37
3.3 a Effects Of Particle Concentration.....	37
3.3 b Effects Of Altering The Shear Rate.....	39

Table of Contents Continued

3.4	<u>Comparisons Between Rigid Spheres And</u> <u>Aggregated Latex</u>	48
	<u>Chapter Four. Conclusion</u>	51
	<u>Chapter Five. Appendix</u>	53
	<u>References</u>	59

List of Figures

Chapter One

- Figure 1. Schematic representation of the energy of interaction between two colloidal particles as a function of the distance between them.4

Chapter Two

- Figure 2. Schematic diagram of experimental setup illustrating the dark field illumination scheme used.18
- Figure 3. Diagram of the three different inter-particle separations calculated by the particle analysis program.21

Chapter Three

- Figure 4. Structure formation that develops with aggregating latex.25
- Figure 5. Change in the mean cross sectional area of aggregates with time after mixing.27
- Figure 6. Change in the mean cross sectional area of aggregates with shear rate.30
- Figure 7. Change in the mean cross sectional area of aggregates with latex concentration.33
- Figure 8. Dependency of the surface separation between aggregates on the mean cross sectional area.34
- Figure 9. Change in the mean cross sectional area of aggregates with salt concentration.36
- Figure 10. Series of photographs showing the effect of shear rate on the ordering phenomenon.42

List of Figures Continued

- Figure 11. Surface separation/diameter ratio vs the particle Reynolds number for the larger beads.44
- Figure 12. Surface separation/diameter ratio vs the particle Reynolds number for the smaller beads.45
- Figure 13. Surface separation/diameter ratio vs the reduced particle Reynolds number.46
- Figure 14. Logarithmic plot of the surface separation/diameter ratio vs the reduced particle Reynolds number.47

List of Tables

Chapter Two

Table I	Properties of the Polystyrene Latex used in the aggregation experiments.	13
Table II	Properties of the polymer microspheres used in the shear flow experiments.	14
Table III	Composition and properties of solutions used to suspend polymer microspheres.	14

Chapter Three

Table IV	Summary of the shear rate regions in which structuring is lost in aggregated latex systems.	29
Table V	Comparison between different particle concentrations. .	38
Table VI	Interparticle separations for different numbers of aligned particles.	39
Table VII	Summary of the shear rates at which structuring is lost in suspensions of neutrally buoyant rigid spheres.	40
Table VIII	Comparison of the surface separations between aggregated latex particles and rigid spheres.	48

Chapter Five

Table IX	The effect of shear rate on the aggregation kinetics. .	53
Table X	The effect of latex concentration on the aggregation kinetics.	54
Table XI	Growth of aggregates with time after mixing.	55
Table XII	Growth of aggregates with time after mixing.	56
Table XIII	Growth of aggregates with time after mixing.	57
Table XIV	Growth of aggregates with time after mixing.	58

Acknowledgements

I would like to thank Dr. Donald E. Brooks for supervising this work, Jim Sibley for his very prompt attention to any of the mechanical problems that occurred with the shearing device, and all the members of the Brooks laboratory for providing a congenial working atmosphere over the last two years. I would also like to thank Peter Easthope for the many, very helpful, discussions we had during the final stages of the preparation of this thesis. Financial support for this work was provided by the User Development Program of the Canadian Space Agency.

CHAPTER ONE

Introduction

In this thesis I will describe and attempt to characterize an ordering effect which occurs when a suspension of particles is sheared in a concentric cylinder shearing device. Instead of adopting random positions throughout the fluid as one might expect, under certain conditions, the particles are found to arrange themselves in regular lines which travel parallel to the direction of flow. This is indeed a surprising result which contradicts the assumption of homogeneity inherent in most of the theoretical treatments of such flows.

Because of the frequency with which dispersions of particles in aqueous media are encountered in everyday life a considerable effort has been made by the scientific community to understand the physical interactions which occur between the particles themselves and between the particles and the fluid which separates them. In many cases the interactions that occur while the suspension is in motion are of primary interest. The flow of blood cells around the body and the behavior of ore and coal suspensions during transportation are just two examples.

The most commonly studied rheological characteristic of dispersions is the shear stress-shear rate relationship, its time and frequency dependence and how these are affected by the material properties of the sample. Data from these types of measurements allow one to calculate the viscosity and hence the energy dissipation rate under different flow conditions. Measurement of the wall shear stress produced at a steady rotational rate in a concentric cylinder or cone and plate viscometer has most often been carried out (1,2) but the shear rate arising from the

application of a constant shear stress (3), the phase and amplitude of the response to an applied oscillatory shear (4) and the propagation velocity of a small amplitude shear wave (5) are also frequently studied. The latter two techniques provide information regarding the viscoelastic properties of the suspensions. Much of the effort in analysis of this type of data has been concerned with determining the inter-particle forces present and indeed great strides have been made in developing theories that explain the observed results for dispersions of low concentrations of uniform particles exposed to low shear rate (6-9).

It has been less common to observe the suspension as shearing occurs, which may explain why the ordering process described here has remained unnoticed for so long. In most cases it has been assumed that the suspended particles adopt random positions within the flow. For some time however, it has been known that highly monodisperse polymer spheres can adopt crystal like structures, both in the absence (10-14), and presence of shear (15,16). Unlike the ordering phenomena I shall describe, structuring is limited to systems for which the inter-particle separations are small enough to be spanned by electrostatic forces. The spheres become charged in aqueous solutions of low ionic strength as a result of the dissociation of protons from acidic groups on their surfaces, and it is thought that the electrostatic repulsion acting via the electrical double layer produces the crystal structures observed. The forces between particles are weak and the application of a low shear stress is usually sufficient to cause melting of the crystals. Ackerson and Clark have investigated the order disorder transitions that occur as the shear rate is increased (16).

The ordering phenomenon, which I have studied, occurs when similar

polymer spheres are allowed to aggregate in the presence of salt. It was first noted in passing by Olal (17). As was stated earlier the spheres possess an electrostatic charge in aqueous media. This charge results in a build up of oppositely charged ions close to the surface of the sphere and what is known as a diffuse (electrical) double layer is formed around each particle. When two particles approach each other, a point is reached where the two double layers begin to interact and a repulsive force results. In all colloidal suspensions these repulsive forces are matched against the London van der Waals attractive forces due to the polarization of one molecule by fluctuations in the charge distribution in a second molecule and vice versa. By combining the equations describing the two opposing forces Derjaguin and Landau (18), and Verwey and Overbeek (19), independently arrived at a theory for colloid stability now commonly referred to as the DLVO theory. In this theory the free energy of interaction between two spherical particles at short separations is given by the following equation:

$$V_{\text{int}} = -\frac{A a}{12h} + C e^{-\kappa h} \quad (1.1)$$

Where: A is a constant known as the Hamaker constant whose magnitude depends on the natures of the material making up the particles and the medium in which they are immersed.

a is the radius of the spheres.

h is the center to center distance between the particles.

C is a constant whose magnitude depends on the magnitude of the particle surface charge density.

κ is a constant whose magnitude is inversely related to the range of the repulsive forces.

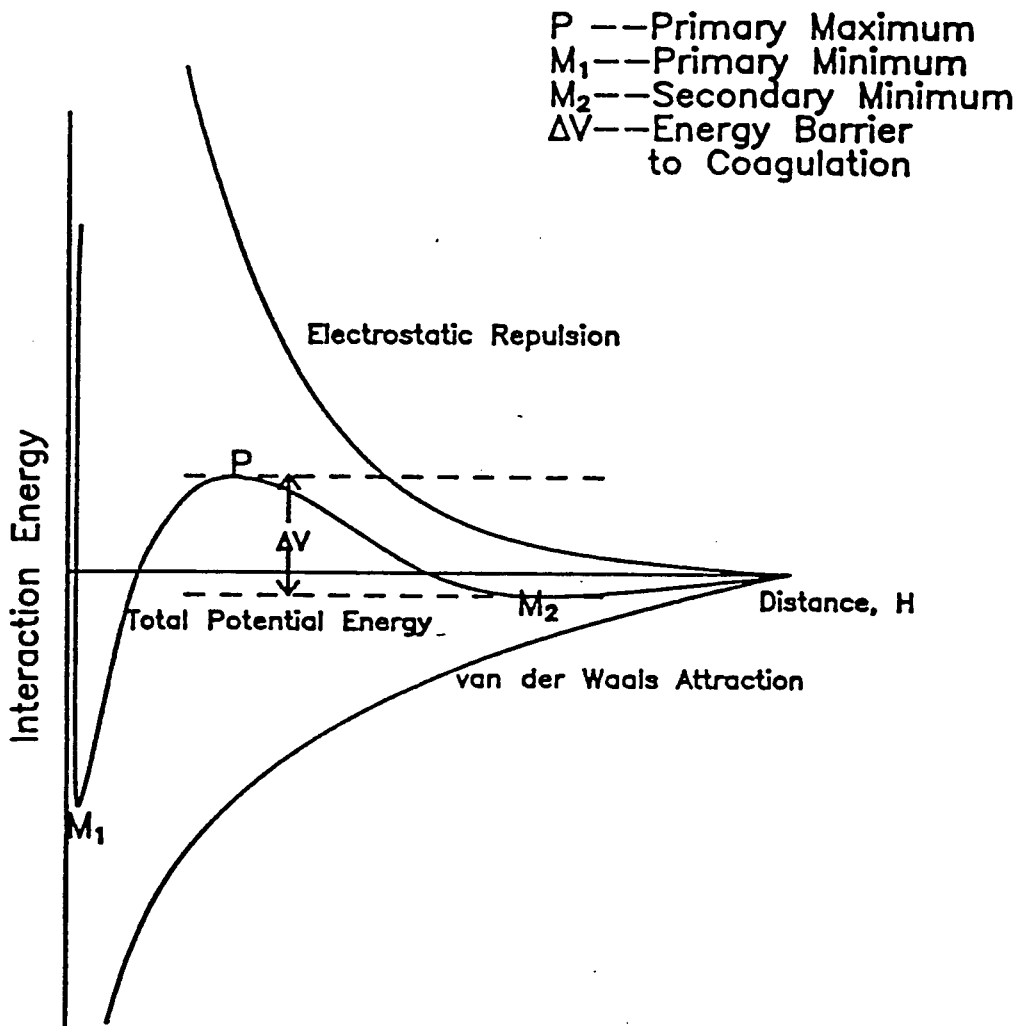


Figure 1. Schematic representation of the energy of interaction between two colloidal particles as a function of the distance H between them. (Adapted from Everett, 20).

Figure 1 illustrates how the free energies of repulsion and attraction combine to give the total free energy curve shown. An additional repulsive term, the Born repulsion has been included, it operates at extremely short distances and prevents the particles from interpenetration. The curve clearly illustrates the energy barrier that is responsible for the stability of the dispersion. The height of the barrier is dependent on both the surface potential, ψ_0 , and the double layer thickness, κ^{-1} . By increasing the salt concentration the thickness of the double layer decreases and at a critical concentration, referred to as the critical coagulation concentration, the energy barrier is reduced enough that coagulation ensues. Although the DLVO theory forms the basis of colloid stability theory extensions have been made to account for additional forces which may be acting. For example in the presence of adsorbed polymer the possibility of steric stabilization must be considered.

In the present study alignment of particles only begins towards the later stages of the aggregation process when the aggregates have grown to a reasonable size. Interactions are seen to occur between particles separated by several mm; over these distances all colloidal forces become negligible. It therefore seems likely that longer range hydrodynamic interactions must be present and that a careful study of fluid motion will be required in order to understand the physical processes which result in this most unusual ordering phenomenon. For this reason, in the remainder of the introduction, I will attempt to summarize what is currently known about flows within such particulate suspensions.

Before presenting this review it is necessary to introduce the two fundamental equations which describe the motions of fluids, namely, the

continuity equation and the Navier-Stokes equation. The continuity equation is derived by applying the principle of conservation of mass to a small stationary volume element within a flowing fluid. Its vector form is given below for an incompressible fluid with constant density:

$$\nabla \cdot \mathbf{v} = 0 \quad (1.2)$$

Where: \mathbf{v} is the local average fluid velocity.

∇ is the differential operator.

The Navier-Stokes equation may be obtained by applying Newton's second law to small stationary volume element within a fluid. According to this law, the sum of the forces acting on the element are equal to the product of its mass and the acceleration it receives. The vector form of the Navier-Stokes equation for an incompressible Newtonian liquid in the absence of any external forces is:

$$\rho \left(\frac{\delta \mathbf{v}}{\delta t} + \mathbf{v} \cdot \nabla \mathbf{v} \right) = -\nabla p + \mu \nabla^2 \mathbf{v} \quad (1.3)$$

Where: ρ is the density of the fluid.

μ is the viscosity of the fluid.

p is the hydrostatic pressure.

Generally one would like to solve equations (1.2) and (1.3) in order to obtain the pressure and velocity distributions within the fluid. To do this the boundary conditions must be specified. For flow around

particles, the fluid velocity is assumed to be equal to the undisturbed velocity far from the particle and to be zero at the surface of the particle. Unfortunately however, due to the non-linear nature of the Navier-Stokes equation, solutions are only available for the simplest of flow systems. Important simplifications can be made to the Navier-Stokes equation for two extremes in the flow regime. This is most easily demonstrated by expressing the Navier-Stokes equation in terms of the dimensionless parameters:

$$x' = x/l ; \mathbf{v}' = \mathbf{v}/v_0 ; p' = lp/\mu v_0 ; \text{ and } Re = lv_0\rho/\mu$$

The primes indicate dimensionless values and,

l is a reference scale length.

v_0 is a reference velocity.

Re is the Reynolds number which can be interpreted as the ratio between the inertial and viscous forces.

Using dimensionless parameters the Navier-Stokes equation then becomes:

$$Re \left(\frac{\delta \mathbf{v}'}{\delta t'} + \mathbf{v}' \cdot \nabla' \mathbf{v}' \right) = - \nabla' p' + \nabla'^2 \mathbf{v}' \quad (1.4)$$

When $Re \gg 1$ the terms on the right hand side of equation (1.4) can be neglected. This type of flow is called inviscid or potential flow since it results from neglecting the viscous terms of the Navier-Stokes equation. This approximation is commonly used to calculate the flow profiles of parts of the fluid remote from the surface of the solid or

outside of the boundary layer where viscous forces are significant. Above a critical Reynolds number, the magnitude of which depends on the geometry of the system, the flow becomes turbulent and statistical laws must be used describe it.

The other extreme occurs when $Re \ll 1$; this is referred to as the Stokes or creeping flow regime. This type of flow is characterized by either slow motion around a body or motion around very small particles. Viscous terms predominate over the inertial terms and the Navier-Stokes equation reduces to the following:

$$\mu \nabla^2 \mathbf{v} = \nabla p \quad (1.5)$$

Detailed analysis has been possible for the flow around particles undergoing shear in the creeping flow regime and the streamlines (imaginary lines which are everywhere tangent to the fluid velocity vector) around such particles have been calculated for single spheres (21), for two spheres in the absence of other external forces (22,23), for two spheres subject to van der Waals forces (24), and for two electrically charged spheres (25). The hard sphere solution predicts that the streamlines are either open or closed according to whether they lie outside or inside the so called limiting streamline. The distance of closest approach of two spheres is limited by the distance between this limiting streamline and the surface of the sphere, it is found to be smallest for similar sized spheres (24). When van der Waals and electrostatic forces are present there are no longer any closed trajectories and the possibility exists, in the presence of a net attractive force between the two spheres, that one sphere will become

captured in the presence of another around which it begins to orbit (26,27).

Unfortunately most of the work described in this thesis is carried out in flows where the Reynolds number is too large for the creeping flow approximation to be applicable. Far less attention has been given to flows with Reynolds numbers above one and below the value for which the onset of turbulence occurs. This is especially true for particles undergoing shear. The flow of a fluid around a stationary particle however, is fairly well understood in this region. Calculations have been made using the boundary layer model which assumes that the flow is inviscid in all but the small region lying close to the surface of the particle. The velocities and pressure distributions can be calculated in the inviscid regions using the potential flow equation. If the boundary layer is thin its presence will have little effect on the flow pattern near the body. For flow around a stationary sphere the streamlines become increasingly asymmetric with increasing Reynolds number but continue to follow the contours of the sphere until at a particle Reynolds number of about 20 (29,30) separation occurs and recirculating wakes is formed behind the sphere. Both theory and experiment indicate that the wake widens and lengthens with increasing Reynolds number (30). Since separation results from the drop in pressure which occurs between the front and back of the sphere, the shape of the particle and hence the nature of the pressure drop strongly influence wake formation. In general the wake volume decreases as the body becomes more streamlined (30). Surface roughness has also been found to affect the nature of the wake. By promoting turbulent flow within the boundary layer, surface roughness delays the formation of a wake and decreases its volume (31).

The type of flow of specific interest in the present context, i.e. moderate Reynolds number flow around particles undergoing simple shear, appears to be one of the least well understood. The problem is complicated by the fact that the particles rotate as a result of the shear forces within the fluid. Poe and Acrivos (32) have measured the rates of rotation and with the aid of tracer particles, photographed the streamlines around single cylinders and spheres freely suspended in a Newtonian fluid undergoing simple shear. Their results show that the angular velocity of the particles in the presence of inertial forces is lower than the value of $0.5 G$ (where G is the velocity gradient) which is expected for $Re \ll 1$ (21). Furthermore their results show that difference between the measured value of the angular velocity and the value given by the creeping flow solution, increased with the Reynolds number though this effect was smaller for the spheres than for the cylinders. The streamline photographs indicate that each body is surrounded by a region of closed streamlines followed on either side by two stagnation points which are in turn followed by two recirculating wakes. As the Reynolds number increased it was found that the distance between the stagnation point and the surface of the body decreased. These results give some indication of the type of flow pattern that might exist in the present context. Unfortunately however, no similar study appears to have been conducted using systems containing several interacting spheres, and so one is left to speculate as to what the flow pattern might look like in these situations.

In the published literature the only effect which bears any resemblance to the structuring phenomena I shall describe occurs as a result of the "tubular pinch effect" first described by Segré and

Silberberg (33-35). This effect is the inertia-induced lateral migration of small suspended particles which can be observed in flowing suspensions. For Couette flow, neutrally buoyant rigid spheres migrate to a location mid-way between the walls, while for both two and three dimensional Poiseuille flow the sphere ultimately attains an equilibrium position which is approximately 60% of the way from the center-line to the vessels walls (35). Migration is thought to occur because of the lateral force the spheres feel as a result of their circular motion within the shear field. Whilst performing their experiments Segré and Silberberg noted the existence of what they called "necklace-like formations of particles" which were presumably the result of interactions between particles in the region where they had migrated as a result of the tubular pinch effect. Segré went on to investigate this effect and reported that their frequency of occurrence depended linearly on particle concentration and dimension (36), and Bauckhage (37) noted that the mean separation between the spheres which make up a single line was a function of the Reynolds number and the number of particles in the line. Neither author however provided a satisfactory explanation for the formations they observed and neither reported the existence of such ordering in the cylindrical shearing device used in this thesis.

By observing the ordered lines through the walls of a cylindrical Couette shearing device the task of photographing the particles is made much simpler. In order to gain insight into the underlying hydrodynamic forces which give rise to this remarkable phenomenon, particle-particle separations have been measured and comparisons are made between numerous different systems. Perhaps the most original work in this thesis comes from the comparisons which are made between the ordered lines observed

with the aggregated latex systems and those which are observed with rigid spheres.

CHAPTER TWO

Experimental Methods

2.1 Preparation Of Latex And Solid Bead Suspensions

Monodisperse polystyrene latex synthesized without surfactant was obtained from Interfacial Dynamics Corporation, Portland, OR. The 8.4% w/w suspension supplied by the manufacturers was centrifuged and resuspended in distilled water before finally being made up into a 1% w/w stock solution. Latex concentrations were confirmed by weights recorded before and after drying in an oven at 60-80°C for 24 hours. Some of the physicochemical properties of the polystyrene Latex used in the aggregation studies are summarized in Table I.

Table I

Properties of the Polystyrene Latex used
in the aggregation experiments

Latex Type	Diameter (nm)	Surface Charge Density (μCcm^{-2})	Density (g/ml)	Critical Coag. Conc. (moles/l)
Sulphate	1073±5.04%	- 6.70	1.055	0.15

In the majority of the aggregation studies the latex solution was mixed in equal proportions with 2.88 M NaCl, resulting in a final salt concentration of 1.44 M, the concentration of sodium chloride which has virtually the same density as the polystyrene latex at 20°C.

To investigate the effects of shear flow on suspensions of larger rigid spheres, uniform polymer microspheres were obtained from Duke Scientific Corporation, Palo Alto, California. The properties of the two different types of sphere used in the experiments are summarized in Table II.

Table II
Properties of polymer microspheres
used in shear flow experiments

Microsphere Composition	Diameter(μm)	Colour	Density(g/ml)
Polymethylmethacrylate	1059 \pm 21	White	1.19
Polystyrene Divinylbenzene	539 \pm 11	Clear	1.05

Table III
Composition and properties of solutions used to suspend
polymer microspheres.

Main Components	Density (g/ml)	Viscosity (mPa s) (25°C)
Sucrose/Water	1.051	1.31
Sucrose/Water	1.060	1.42
Ethylene Glycol/Water	1.060	2.94
Sucrose/Water/Ethanol	1.060	10.80
Glycerol/Ethanol	1.060	25.49
0.1 M NaCl	1.002	0.91
1.44 M NaCl	1.055	1.03
2.0 M NaCl	1.077	1.09

In every case the density of the suspending media matched the density of the beads. A variety of viscosities were used and small amounts of sodium dodecyl sulphate were also added to the suspending medium to improve the wetting properties of the otherwise hydrophobic beads. The composition and properties of the various suspending media are summarized in Table III.

2.2 Experimental Apparatus And Arrangement

The experiments were performed in a concentric cylinder shearing device specifically designed for this purpose. The device comprised of an outer, rotating, precision bore pyrex cylinder (height 4.8 cm, 7.74cm inner radius) and a stationary solid plexiglass inner cylinder. Two different inner cylinders were used with radii of 7.59 cm and 7.44 cm, giving gap widths of 0.15 cm and 0.3 cm respectively within which the sample was sheared. The angular velocity, Ω , of the outer rotating cup was calculated by measuring the time, Δt , required for a line drawn on the outer surface of the cup to make N revolutions. A mean value of Ω for the cup at each particular shear rate was then calculated by averaging three separate measurements of $N/\Delta t$ (the standard deviation was usually lower than 0.1%). The shear rate, G , at distance r from the axis of the cylinders was calculated from the following expression (38):

$$G = 2 \Omega \frac{1 / r^2}{1 / R_b^2 - 1 / R_c^2} \quad (2.1)$$

Where :

R_b = radius of bob (inner cylinder)

R_c = radius of cup (outer cylinder)

All of the shear rates quoted in this thesis are calculated for the flow at the center of the gap i.e. by putting, $r = (R_c + R_b)/2$, into the above expression.

Three different motors were used to drive the outer cylinder, the first, a 7 rpm 1/30 hp D.C. gear motor (Dayton) gave shear rates in the range $0.1-21 \text{ s}^{-1}$ (for the smallest gap width) within which the majority of experiments were carried out. The two other motors used had speeds of 21 rpm and 102 rpm making it possible to examine rates in the range $0.1 \text{ s}^{-1}-320 \text{ s}^{-1}$ (for the smallest gap width). In all cases the motors were controlled by a precision control to which they were coupled by a multiple O ring pulley.

When studying the salt aggregated latex systems, the suspension was loaded into the gap between the cylinders through a small hole drilled near the top of the inner cylinder which was in turn connected to a filling nipple. The polystyrene latex suspension in distilled water and the concentrated salt solution were contained in two separate 60 ml syringes. These syringes were connected via polyethylene tubing to a mixing T-joint from which a third length of tubing ran to a 3-way tap which had one outlet to the filling nipple and one to a beaker for collecting waste solution. The syringes were expressed simultaneously with a dual syringe pump at about 41 ml/min. By using the 3-way tap, solution could be pumped through the system to waste for a couple of seconds before being switched to deliver into the shearing device. In this way any air trapped within the system was expelled before the

suspension was introduced into the gap. Mixing of the latex and salt solutions produces aggregation conditions but the high shear rates in the tubing were thought to minimize any aggregation in this location. The latex was exposed to uniform shear flow approximately 2.5 s after being mixed with the salt. This interval is small on the time scale of the reaction of interest. When studying the solid sphere suspensions these were introduced into the gap manually with a dropping pipette when the outer cylinder was in motion.

The cylinders were oriented vertically and the suspensions were observed horizontally with a Zeiss Tessovar Photomacrographic Zoom system and the images were recorded using a Nikon F3 camera mounted on the lens. Typically a magnification of 1.6 times was used to image an area of approximately 2.4 cm by 1.6 cm. At this magnification the depth of field, for the aperture of 4 used, was 1.3 mm (manufacturers figures). This meant that the majority of the gap could be kept in focus at the same time. The dark field illumination scheme, illustrated in Figure 2, was found to give the optimum results. A cylindrical mask extended about the top of the outer cylinder and behind this a flash unit was mounted with its beam orientated so that it pointed down into the gap containing the suspension. The mask prevented light from entering the lens directly. The latex suspension or polystyrene beads scattered light into the lens registering as bright spots on the photographic emulsion. To increase the contrast between the latex and the inner wall of the Couette device, the inner cylinder was painted black. 400 ASA TMAX film was used to record the images and this was processed with Kodak HC110 developer using the process recommended by the manufacturers. Prior to each run a metal rule was placed into the field of view and a photograph was taken.

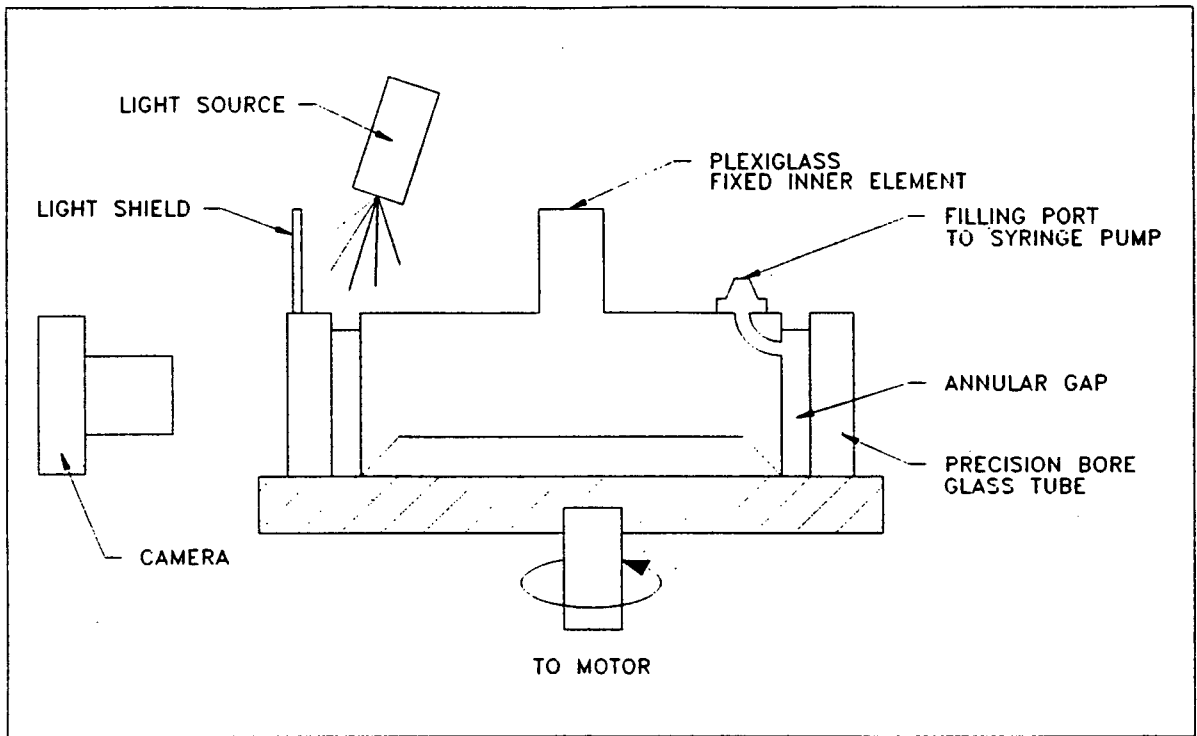


Figure 2. Schematic diagram of experimental setup illustrating dark field illumination scheme used.

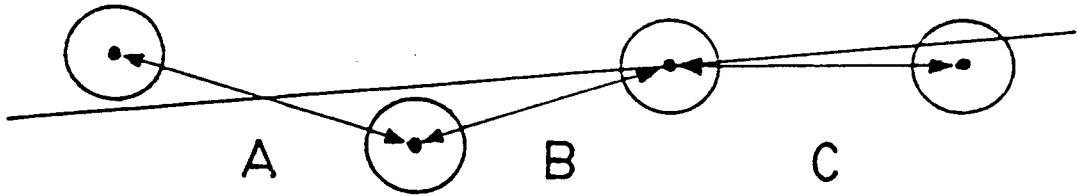
The scale recorded was then used to calculate the scale factor for the image analysis program.

2.3 Image Analysis

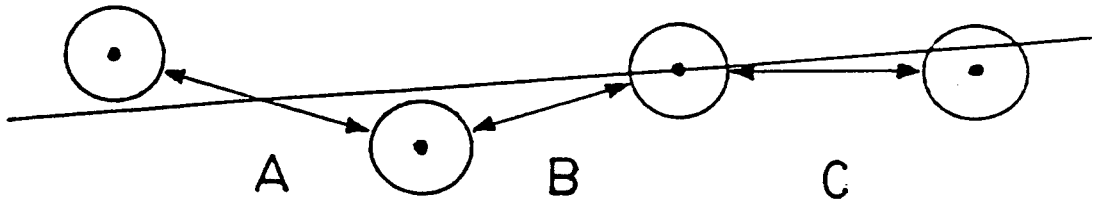
Once processed the negative images were stored and analyzed with an I.T.I. P.C.-Vision Plus frame grabber mounted in a Everex 386 32 bit computer equipped with a 387 coprocessor. This frame grabber accepts a 640 by 480 array in 1/30 s. Before any analysis was attempted a specially developed program was used to minimize variations in light intensity by enhancing regions with large gradients in light. After the image had been corrected for variations in light intensity, it was analyzed using a second particle analysis program. In this program every pixel of the array is scanned to identify particles with intensities below a set threshold value. Once a dark pixel has been located a sub-routine within the program utilises an algorithm to trace the outline of the particle before the scan of the array is resumed. Having located each of the particles within the array the program computes the perimeter, the area, and the center of mass of each particle. The data is displayed in the form of histograms showing the particle size distribution along with the relevant statistics. Particles within a particular size range or individual particles (up to a maximum of 50), can then be selected, for further analysis. A program was also developed to give information about the geometry of aligned particles. This program will determine mean separations between a series of selected particles and vertical distances between the horizontal bands of aligned particles. The program calculates three different inter-particle separations for each line of

particles selected; these are illustrated in Figure 3. Unless otherwise stated the inter-particle separations given in this thesis are surface separations illustrated in Figure 3 (ii). For each of the mean distances calculated the program gives the standard deviation and coefficient of variance. The program also calculates the regression on the best straight line drawn through the centers of the selected particles and the vertical distance separating different lines of particles.

(i) Center Separation



(ii) Surface Separation



(iii) Point Separation

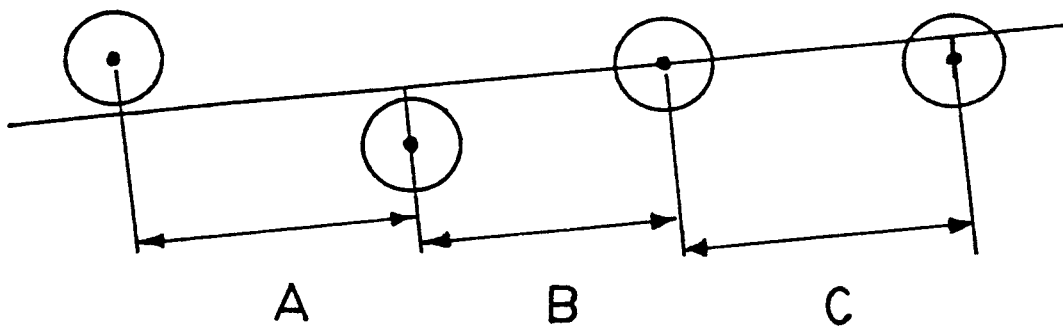


Figure 3. Diagram of the three different inter-particle separations calculated by the particle analysis program for each set of aligned particles selected. Mean separation = $(A+B+C) / 3$ in each case.

CHAPTER THREE

Results and discussion

3.1 a. Introduction To Dimensionless Parameters

For each experiment performed the particular set of conditions used is unique. Before it is possible to establish trends within a system therefore, all of the controllable parameters must be systematically varied. In many cases this can result in an enormous amount of work and it is therefore important to be able to extend and generalize all of the information obtained from each experiment. This goal has been commonly achieved by employing the method of dimensional analysis. In dimensional analysis the number of variables that have to be compared is reduced by grouping them together in dimensionless ratios, in this way several different parameters can all be compared using one dimensionless ratio.

The Reynolds number, previously mentioned in the Introduction, is the dimensionless parameter of most interest here and is simply the ratio between the inertial and viscous forces within the system. The definition of the Reynolds number depends on the length scale and velocity being considered. The Reynolds number I will most often refer to is the particle Reynolds number, resulting from the ratio of the forces experienced by the suspended particles in the flow. The particle Reynolds number is defined by the following equation:

$$\text{Re}_p = \frac{\rho G a^2}{\mu} \quad (3.1)$$

Where: ρ = density of the suspending medium.

G = shear rate (velocity gradient).

a = particle diameter.

μ = viscosity of the suspending medium.

It is possible to define a second Reynolds number for the shear system described, whose magnitude is determined by the ratio of the inertial and viscous forces experienced by the fluid in the annulus of the shearing device. The mean flow Reynolds number is given by the following equation:

$$\text{Re}_f = \frac{\rho v l}{\mu} \quad (3.2)$$

Where: v = velocity of rotating cup

l = gap width

The magnitude of the Reynolds number indicates the type of flow experienced, lower numbers being associated with steady flow and higher numbers being associated with unstable or turbulent flow. In simple tube flow, for example, the flow does not become turbulent until the Reynolds number, based on the tube diameter, exceeds 2100. The particle Reynolds number determines the nature of the flow of the suspending medium around the particle, while the mean flow Reynolds number indicates the type of flow occurring within the annulus of the shearing device. Fortunately, for the shearing device used in this work with the outer cup rotating, laminar flow is strongly stabilized by centrifugal forces. As a result,

transition to turbulent flow takes place at much higher Reynolds numbers than in the corresponding case where the inner cylinder is rotating (41). The mean flow Reynolds number range of 50-700, covered in this work lies well within the region for which laminar flow is expected.

The two other dimensionless ratios mentioned in the following discussion are both ratios of two relevant lengths. These are the diameter ratio, ϵ , which is the ratio of the aggregate diameter to the gap width, and the separation ratio, δ , which is the ratio of the surface separation between aligned aggregates and the mean aggregate diameter.

3.1 b. Error Analysis

Unless otherwise stated the errors quoted throughout this thesis are the population standard deviations (S.D.). For the set of numbers x_1, \dots, x_n , the population standard deviation is defined as follows:

$$\text{S.D.} = \sqrt{\frac{1}{N} \sum_{i=1}^N (x_i - \bar{x})^2} \quad (3.3)$$

Where \bar{x} is the average of the N numbers.

3.2 Salt Aggregated Latex

Figure 4 shows a typical example of how the structuring phenomenon develops when a polystyrene latex suspension is mixed with sufficient salt to cause aggregation and the mixture is sheared. Immediately after mixing the system is cloudy and the particles randomly dispersed. As shearing is continued, however, small aggregates begin to form due to collisions taking place between particles on adjacent streamlines.

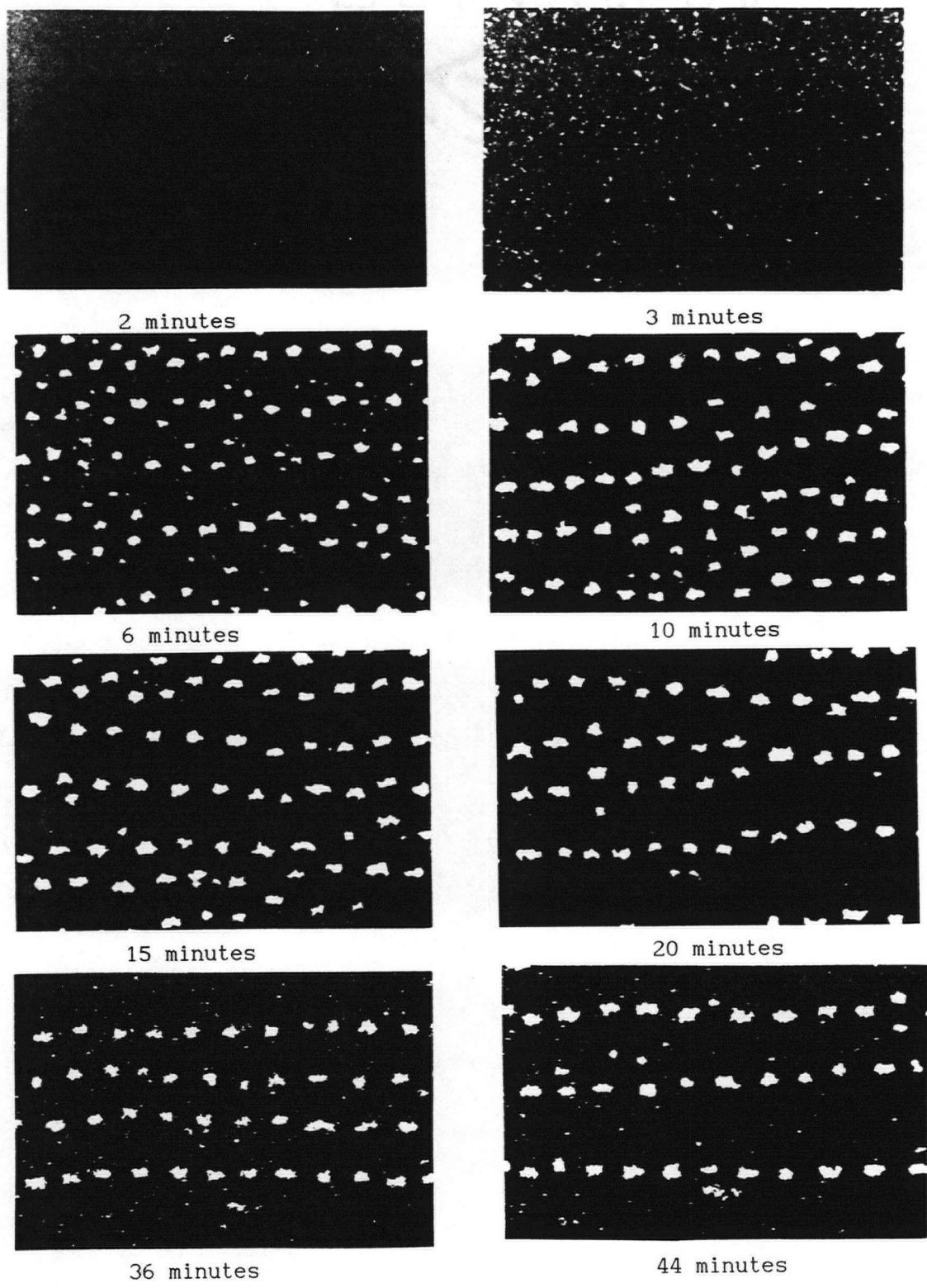


Figure 4. Structure formation that develops when sulphate latex is coagulated with 1.44 M NaCl in a shear field of 21.4 s^{-1} at room temperature. Time elapsed after mixing shown below each frame.

The aggregates continue to grow as more and more single spheres and small clumps are collected into the growing mass. Simultaneously, the visible aggregates begin to align themselves in the direction of the shear flow, forming strings of particles which are separated by an approximately uniform distance. As the particles are translated in the direction of the flow, they also rotate about their centers of gravity as a result of the velocity gradient present within the gap of the shearing device.

Figure 5 shows how the mean aggregate area changes with time after mixing. Initially the aggregates grow quite rapidly but eventually a steady state is reached, presumably when the shear-induced aggregate degradation balances aggregate growth. In some cases a plot of aggregate size vs. time has indicated a decrease in the mean aggregate size after the steady state is reached. These changes are thought to be due to particles sedimenting or creaming (rising) from the field of view because they are not truly neutrally buoyant. In order to make comparisons between systems I have defined a steady state as being the time at which the largest mean aggregate size is recorded during the course of a run. This is a fairly arbitrary assignment so any results from this type of comparison can only be used in a qualitative manner. Aggregate diameters, where quoted, have been calculated as the diameter of the circle of area equal to that measured for the aggregate. Once again this is an approximation, but since on the whole the aggregates are ellipsoidal, with each photograph containing a random selection of projections, this was thought to be the simplest and most effective comparative dimension to use.

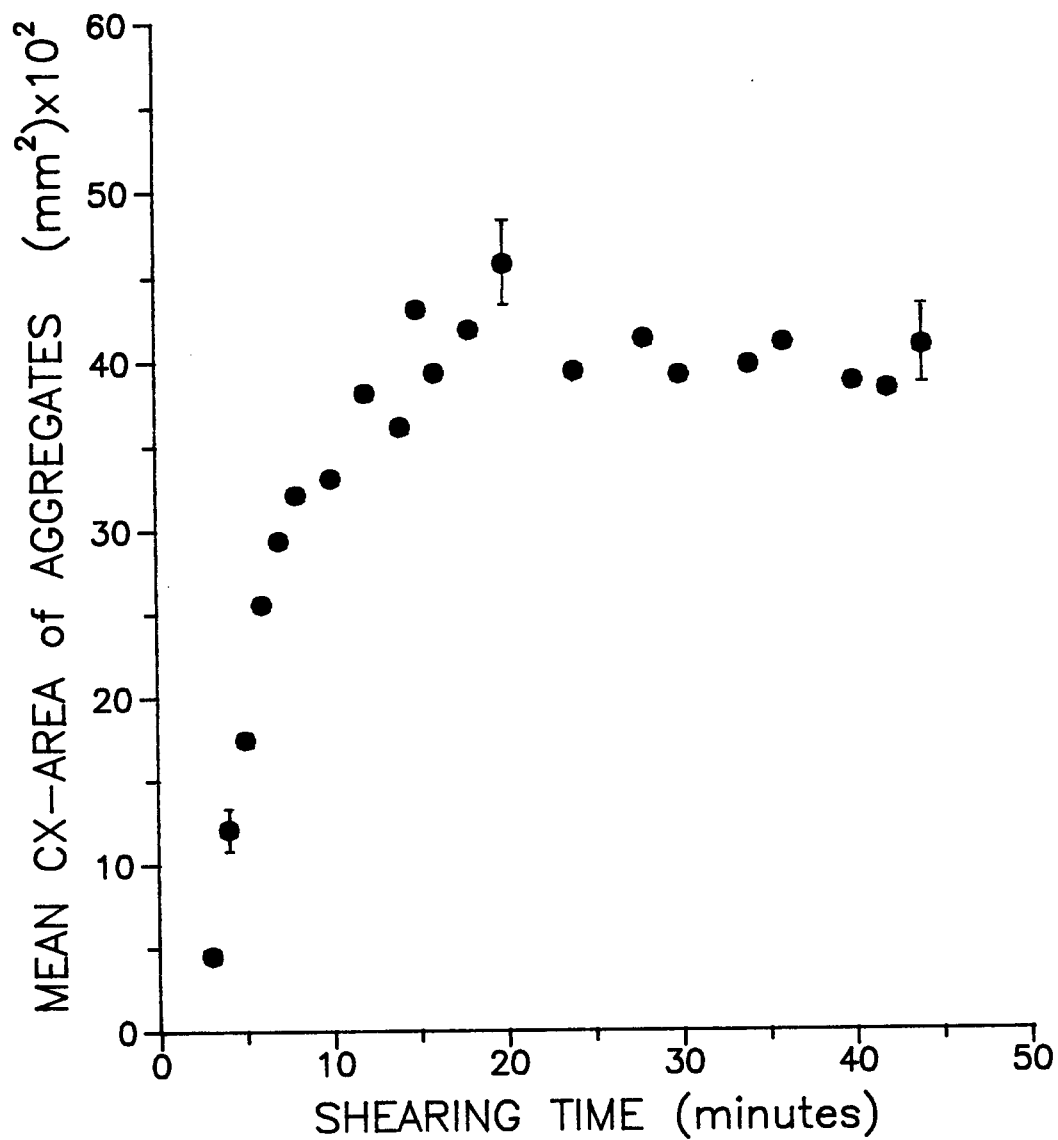


Figure 5. Change in the mean cross sectional area of aggregates with time after mixing. (Shear rate 21.4 s^{-1} , latex concentration 0.05%, NaCl concentration 1.44 M, gap 1.5 mm). Errors are plotted as \pm standard error of the mean.

The conditions used to demonstrate the structuring effect in Figure 4 were chosen to illustrate what happens in a typical run; clearly by changing any one of the initial conditions a different result will be obtained. In the following sections one of the starting conditions is varied while the others are held constant in order to examine exactly the effect a particular parameter has on the phenomenon. This procedure also allows a better definition of the conditions under which the effect is observed.

3.2a Effects of altering the shear rate.

The results from the series of experiments in which only the shear rate was changed indicate that the ordered lines observed become more regular as the rate of shear is increased. At low shear rates ($\leq 5s^{-1}$), although aggregate alignment still occurs the lines are poorly defined and the aggregates grow to the size of the gap and form "clots" which disturb the flow pattern and make investigation difficult. The effect of increasing the shear rate is also complicated by the fact that the resulting shear stresses increase aggregate erosion and so reduce the steady state aggregate size. Figure 6, which shows a plot of the mean aggregate area vs the shear rate, illustrates this effect clearly. As the shear rate is increased the mean aggregate area becomes smaller and smaller. Eventually aggregate ordering is no longer observed. This occurs at different shear rates for the two different Couette geometries studied. These results are summarized in Table IV.

Table IV

Summary of the shear rate regions in which structuring is lost

Ltx. Conc.=0.05%; Sodium Chloride Conc.=1.44M

Gap Width (mm)	Shear Rate (s^{-1})	Diam.(mm)	Diam./Gap	Re _p
<u>Shear Rates Below Which Ordering Observed</u>				
1.5	31	0.47	0.31	1.75
3.0	11	0.94	0.32	2.5
<u>Shear Rates Above Which No Ordering Observed</u>				
1.5	47	0.35	0.24	1.48
3.0	16	0.46	0.16	0.87

Examination of this table indicates that particle size is an important factor in determining whether or not structuring is observed. The region between the upper and lower shear rate limits of Table IV, i.e. between 31 and 47 s^{-1} for the 1.5 mm gap, represents the grey area in which occasional particle-particle interactions are observed. The particle angular velocity increases as the velocity gradient within the flow increases (32). The table shows that despite the fact that the smaller aggregates are rotating with higher angular velocities than their larger counterparts, for which particle alignment does occur, they do not exhibit ordering. Unfortunately because of the reversibility of the aggregate formation it is not possible to examine whether or not structuring can be achieved with these smaller aggregates at higher shear rates. As was pointed out in the Introduction however, the nature of flow around a particle is influenced by particle size, shape and the relative velocity between particle and suspending medium. Presumably each of

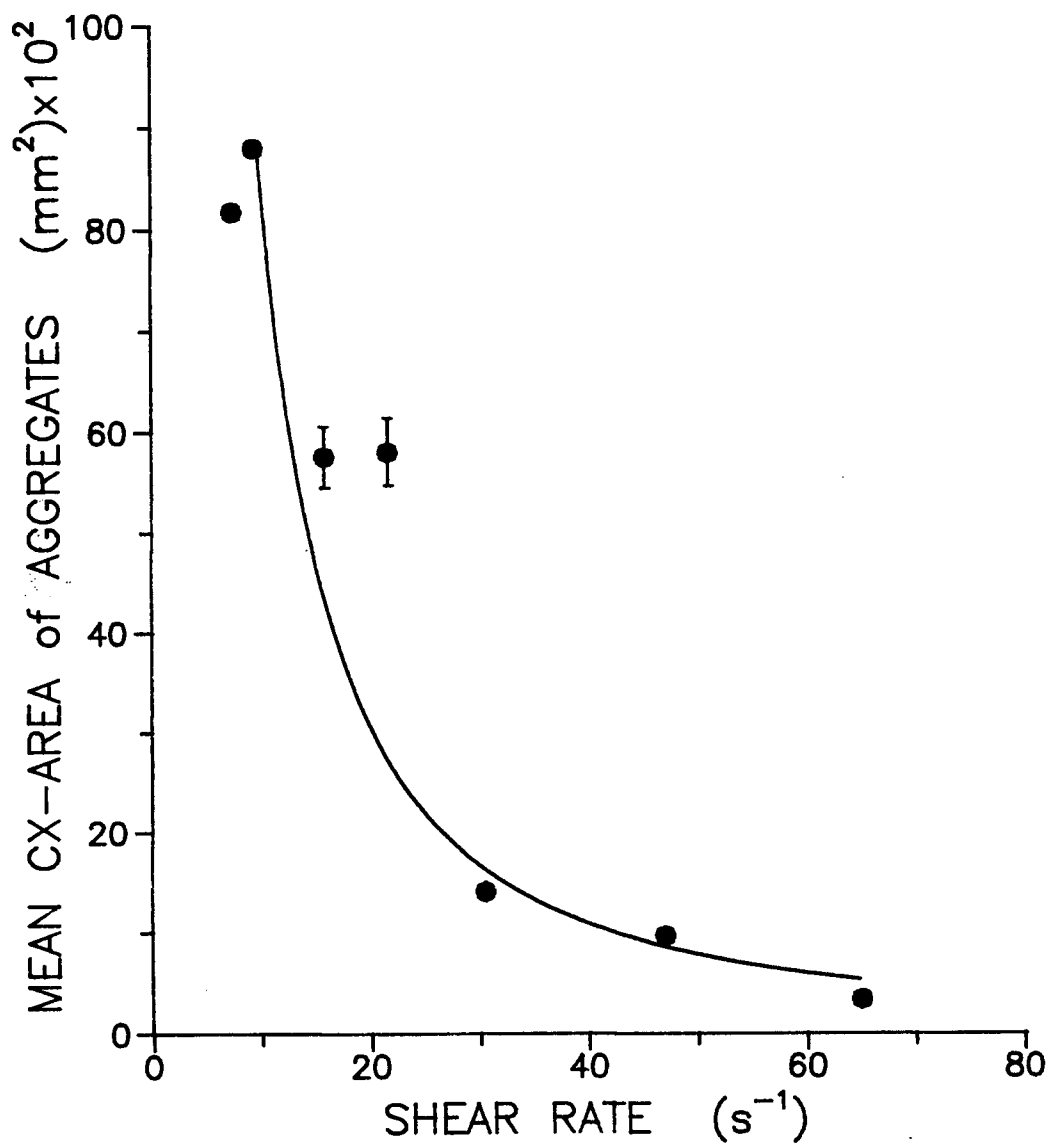


Figure 6. Change in the mean cross sectional area of aggregates with shear rate. (Latex concentration 0.05% w/w, NaCl concentration 1.44 M, gap 1.5 mm). Errors are plotted as \pm standard error of the mean.

these properties will also play a role in determining the nature of the hydrodynamic interaction between particles and thus ultimately whether or not alignment will occur.

Table IV also reveals the importance of the wall effects on the structuring phenomena. It is observed that aggregates with a diameter of about 0.5 mm will demonstrate alignment within a gap of 1.5 mm whereas for a gap of 3.0 mm the structuring phenomena is only observed when larger aggregates are present. Once again this argument is complicated by the fact that comparisons have to be made at different shear rates and so the particles have different angular velocities.

It is clear from the above discussion that any study of the structuring phenomena using aggregated latex particles is complicated by the fact that a change in the shear rate has the dual effect of altering both the size of the aggregates and their angular velocity, in opposite directions. By using rigid spheres to model the system the problem of aggregate erosion is eliminated and the effect of the shear rate becomes much easier to study. Further information on the effects of shear rate on aggregated latex systems is given in Table IX in the appendix.

3.2 b. Effects of changing the latex concentration

A series of experiments were conducted in which only the concentration of polystyrene latex was changed. The shear rate and the salt concentration remained fixed at 7.4 s^{-1} and 1.44 M respectively. This salt concentration was used because it's density matches that of most of the polystyrene latex spheres. Each of the experiments was performed with a gap width of 1.5 mm. Figure 7 summarizes the effect of the latex concentration on the mean steady state aggregate size. As might be expected the mean area of the aggregates increases with an increase in concentration, eventually plateauing when the equivalent aggregate diameter is about 0.74 of the gap width.

The results from this series of experiments can be used to examine the influence of particle size on the structuring phenomenon, since by altering the initial latex concentration one can vary the aggregate size while keeping the particle angular velocity constant. In Figure 8 the surface separation between particles is plotted against the mean aggregate area. The graph demonstrates a clear dependence between the separation of the aligned aggregates and the size of the aggregates. There is a problem here in that the equivalent aggregate diameters range from about 0.3 to 0.7 times the size of the gap. It is therefore difficult to differentiate between the increasing importance of wall effects as the particles grow, and effects due strictly to the increased disturbance of the fluid that is expected for the larger aggregates. Further information on the effect of latex concentration on the aggregated latex systems is given in Table X in the appendix.

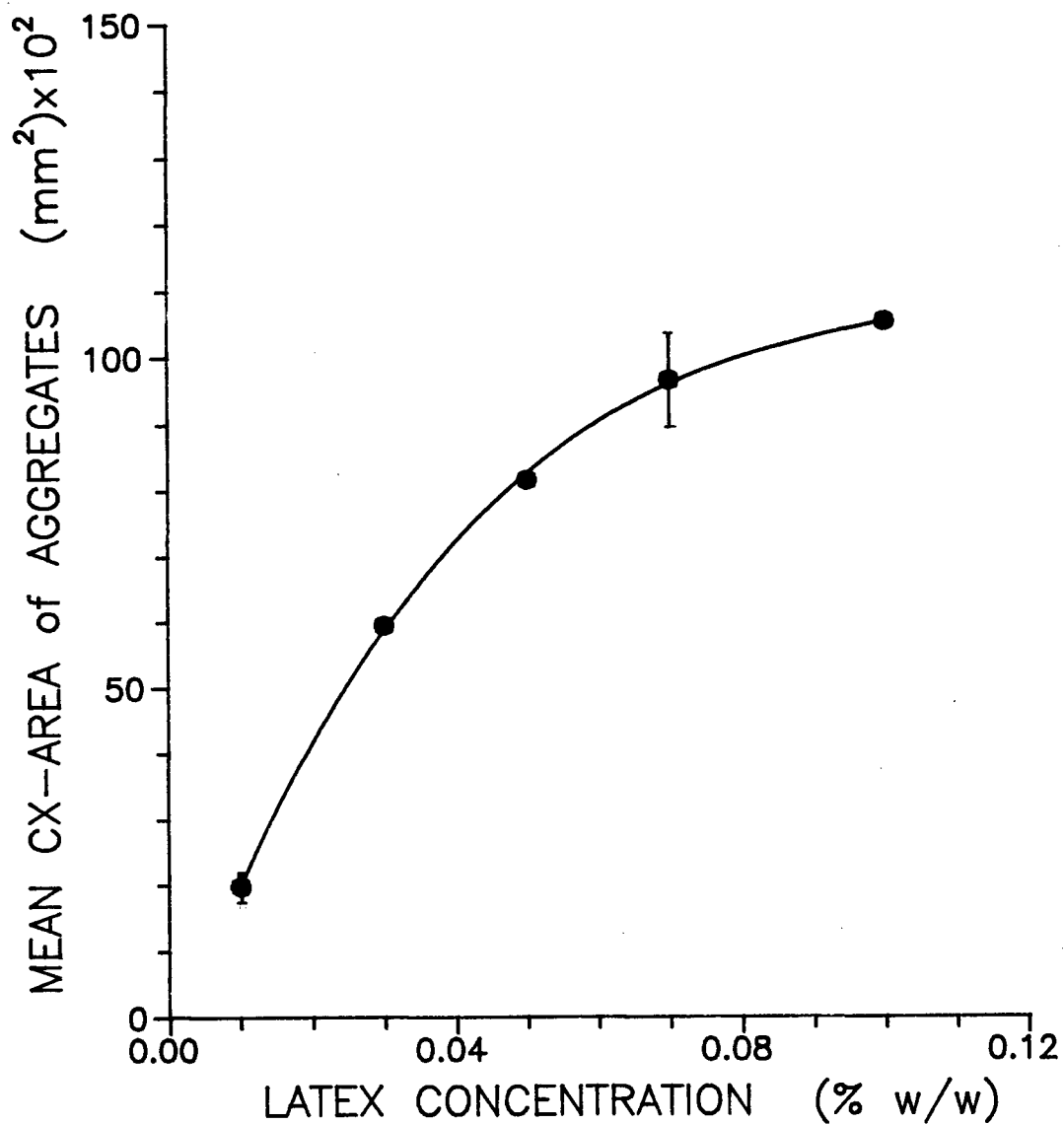


Figure 7. Change in the mean cross sectional area of aggregates with latex concentration. (Shear rate = 7.3 s^{-1} , NaCl concentration = 1.44 M., gap 1.5 mm). Errors are plotted as \pm standard error of the mean.

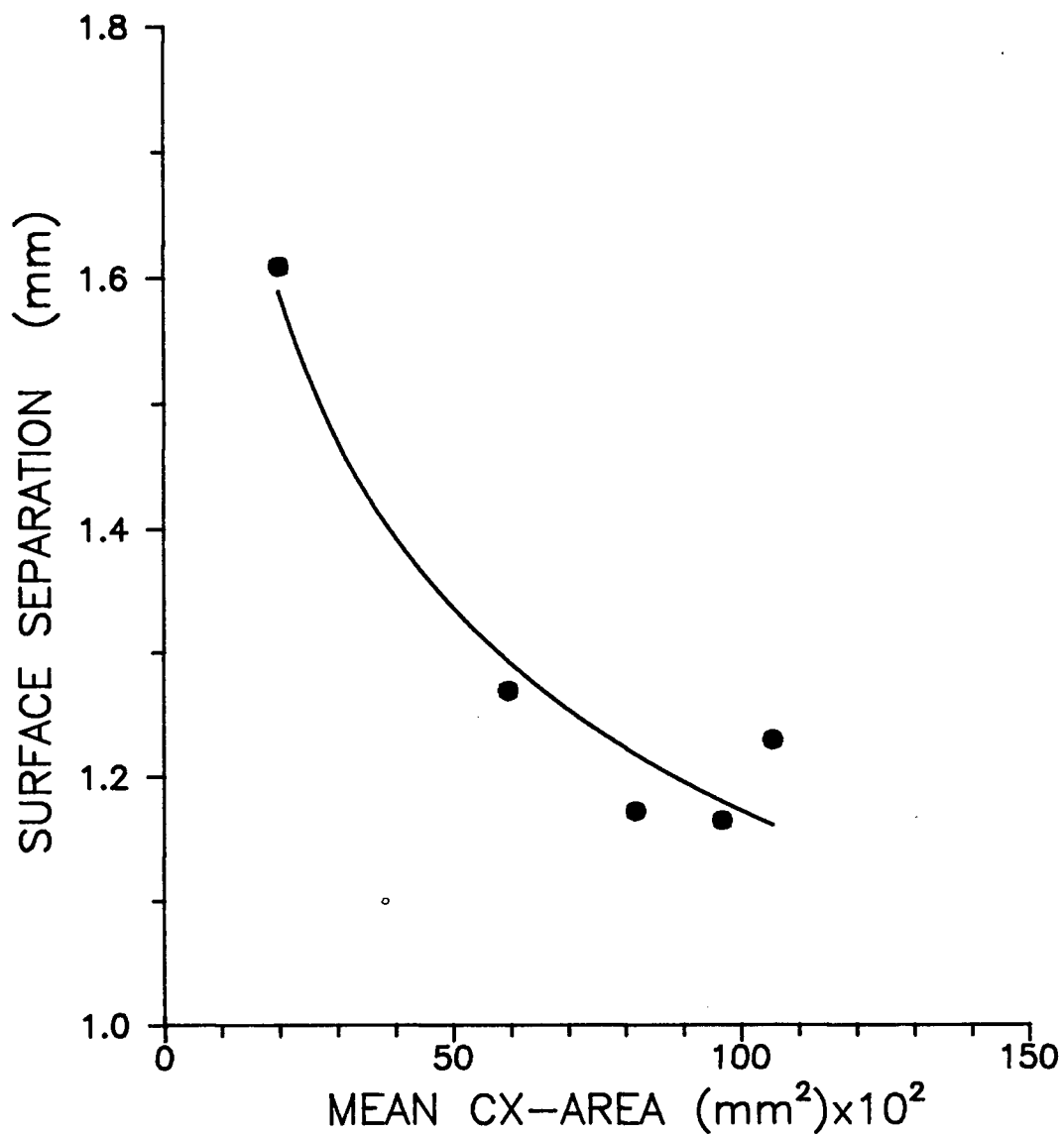


Figure 8. Dependency of the surface separation between aggregates on the mean cross sectional area of aggregates. (Shear rate = 7.3 s^{-1} , NaCl concentration = 1.44 M, Gap width = 1.5 mm)

3.2 c. Effects of altering the salt concentration

The effects of altering the salt concentration at a fixed shear rate of 21.4 s^{-1} and a fixed latex concentration of 0.05% w/w were observed. As can be seen from Figure 9 the mean aggregate area increases with an increase in the salt concentration, reaching a maximum at 1.44 M. The points at 1 M, 1.44 M, and 2 M were shown, by the student t test, to be significantly different. Difference between 1 M and 1.44 M, $t = 4.05$, $N = 70$, $p \leq 0.001$; difference between 1.44 M and 2 M, $t = 2.36$, $N = 54$, $p \leq 0.05$. These results are consistent with colloid stability theory which predicts that an increase in the ionic strength will result in a corresponding decrease in the electrostatic repulsion between the latex spheres. This in turn leads to stronger aggregates that are more resistant to erosion from the shear stresses within the Couette flow and hence which grow to larger sizes. The drop in aggregate size, observed above 1.44 M NaCl, presumably results from aggregates creaming since the isopycnic point has been reached. Upon reducing the salt concentration a point is reached at which the aggregate size is so reduced that the ordering phenomena is no longer observed. For a gap width of 1.5 mm. this is seen to occur at salt concentrations between 0.15 and 0.20 M.

One of the problems associated with studying the system under these conditions is the fact the density of the suspending medium is strongly dependent on the concentration of sodium chloride. Therefore the aggregates sediment or cream depending on whether the salt concentration is above or below 1.44 M, which is the concentration resulting in a roughly isopycnic solution.

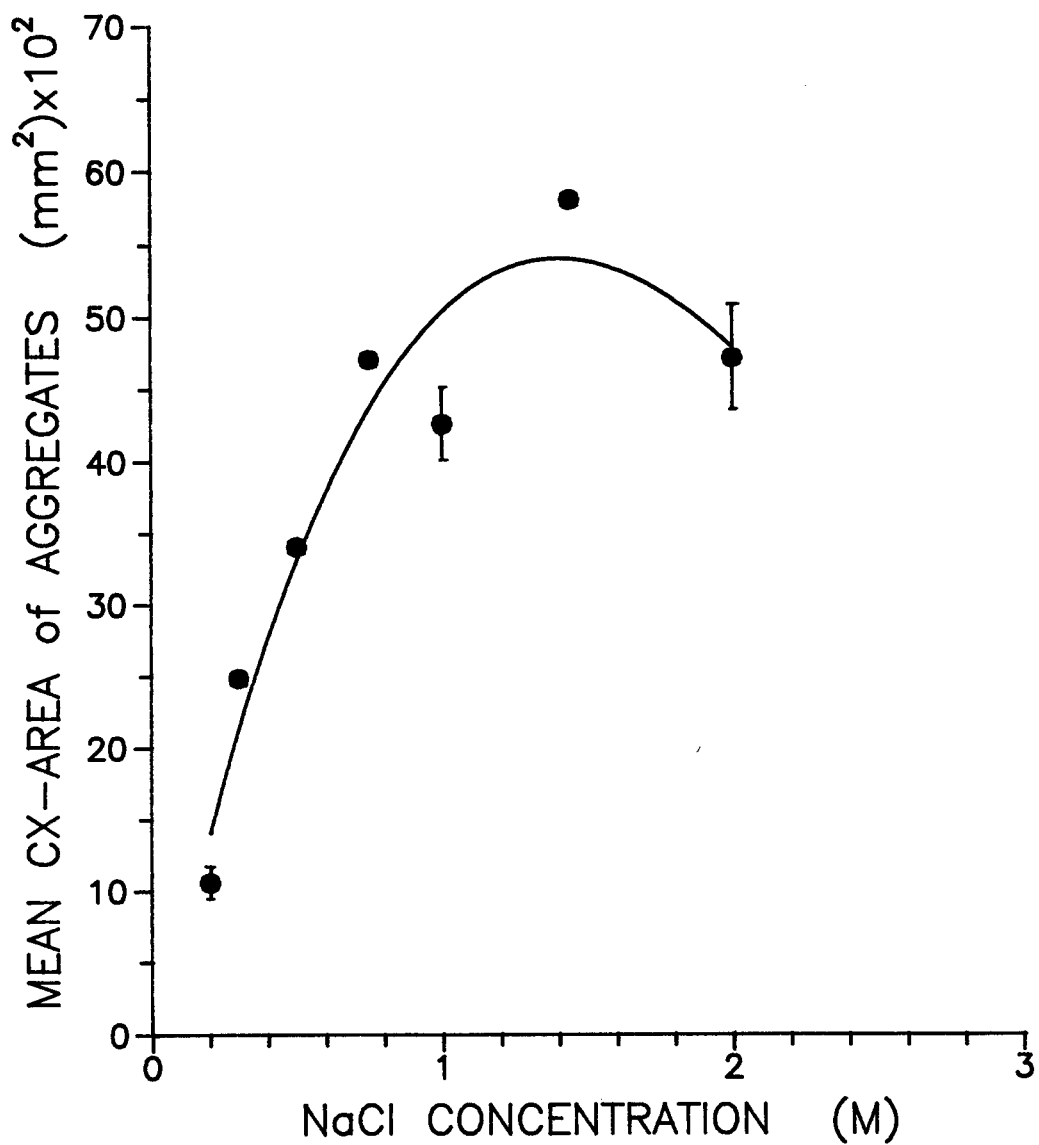


Figure 9. Change in the mean cross sectional area of aggregates with salt concentration. (Latex concentration 0.05% w/w, shear rate = 21.4 s⁻¹, gap 1.5 mm). Errors are plotted as \pm standard error of the mean.

3.3 Rigid monodisperse polymer spheres

The ordering phenomenon described above has also been observed with suspensions of neutrally buoyant rigid spheres. The observation of ordering in suspensions of smooth spheres proves that the irregular surface of the latex aggregates is not a prerequisite for particle alignment to occur. Furthermore the solid beads provided me with a far simpler model with which to study the phenomenon since monodisperse beads whose size has already been accurately determined can be used. In particular the shear rate dependence of the system is a lot easier to study as the size of the beads is independent of the shear stresses they experience. Before presenting the results of the experiments in which the shear dependence of the system is investigated, a brief mention will be given to effects of particle concentration.

3.3a Effects of particle concentration

In Table V the separations between aligned particles are compared for several different particle concentrations. It is clear from the table that within the limits of experimental error the particle separations are independent of particle concentration over the range examined. The inter-particle separations are however affected by the number of beads making up the line, smaller separations being observed for the longer lines. This is illustrated in Table VI below which gives the mean center and surface separations for lines containing different numbers of beads. These results agree at least qualitatively with those obtained by Segré (38) for the aligned beads that he observed when a suspension of particles travelled down the length of tube.

Table V

Comparison between different particle concentrations.

Particle concentration particles/cm ³	Center Separation (± S.D.)	Surface Separation (± S.D.)
<u>Re_p = 1.95</u>		
22.6	3.19±.06	2.04±.07
30.4	3.10±.10	2.02±.14
<u>Re_p = 3.4</u>		
22.6	2.89±.06	1.80±.05
30.4	2.77±.09	1.65±.08
<u>Re_p = 4.5</u>		
5.6	2.80±.06	1.59±.17
9.6	2.66±.01	1.53
13.7	2.58±.22	1.43±.23
22.6	2.71±.07	1.60±.06
30.4	2.78±.10	1.64±.10

Since lines containing different numbers of beads are usually observed in any one particular run, the inter-particle separations quoted in the following sections are the mean separations calculated by averaging the separations measured from lines of various sizes.

Table VI

Interparticle separations for different numbers of aligned particles

Number of beads in line	Center Separation (mm \pm S.D)	Surface Separation (mm \pm S.D.)
2	2.74	1.60
3	2.79 \pm .05	1.66 \pm .04
4	2.75 \pm .06	1.62 \pm .06
5	2.72 \pm .08	1.61 \pm .08
6	2.68 \pm .13	1.53 \pm .17
7	2.66 \pm .01	1.53
8	2.40 \pm .26	1.27 \pm .28

3.3b Effects of altering the shear rate in suspensions of rigid spheres.

In this section the results of experiments studying the effects of the shear rate on the ordering phenomena are presented. Two different geometries were used with gap widths of 1.5 mm and 3.0 mm. In each of these gaps, beads with diameters of 1.059 mm and 0.539 mm were tested, resulting in data for four different diameter/gap ratios, ϵ .

For each of the values of ϵ studied the ordered lines observed become less and less well defined as the shear rate is reduced until eventually there is no longer any interaction between beads. The table below summarizes the shear rates and Reynolds numbers below which structuring is lost in the four different systems studied. Because of the inherent difficulty in defining the point at which ordering disappeared there is likely a considerable amount of error in the figures quoted.

Table VII

Summary of the shear rates at which structuring is lost for
suspensions of neutrally buoyant rigid spheres

Bead Diam. (mm)	Gap Width (mm)	ϵ	Shear Rate(s^{-1}) (structure lost)	Re_p (structure lost)
0.539	3.0	0.18	7	0.4
1.059	3.0	0.355	3	0.5
0.539	1.5	0.362	3	0.2
1.059	1.5	0.71	4	0.8

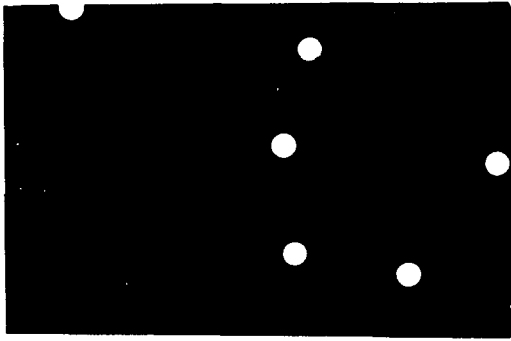
The uncertainties of the figures in the table make it difficult to draw conclusions, although there appears to be no obvious trend going from small to large ϵ . What is interesting, however, is the fact that the ordering phenomenon disappears in all cases for particle Reynolds numbers near one, demonstrating that inertial effects will have to be considered when attempting to explain the particle alignment.

Figure 10 illustrates the effect of increasing the shear rate, below $9 s^{-1}$ there are no particle particle interactions and the beads are randomly distributed throughout the flow. Above $9 s^{-1}$ the effects of hydrodynamic interactions can be seen as particles begin to fall into line. Increasing the shear rate further results in the lines becoming more regular and the inter-particle spacing decreasing. Eventually a point is reached where the separation between particles is so reduced that beads are seen to flip positions with one bead hopping over the other. When this occurs the line is momentarily disrupted but quickly reforms.

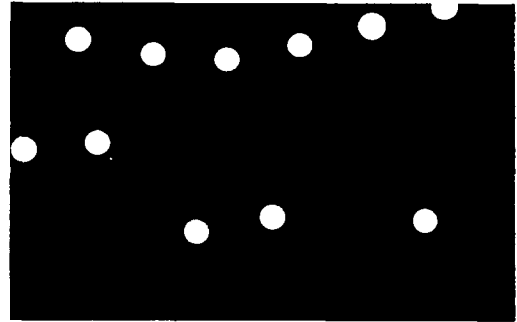
The last plate of Figure 10 shows a disruption that has occurred in a line due to two particles flipping positions. Unfortunately the photographic technique used in this work was not suited to a more detailed study of this process, it would however be informative to employ a cinematographic technique in future work to examine exactly what is taking place at these shear rates.

As was mentioned above, in the shear rate region where particle alignment is observed, the spacing between neighboring beads is seen to decrease as the shear rate and therefore the angular velocity of the particles within the suspension increases; this is clearly illustrated in Figure 11. The graph demonstrates the long range nature of the effect, with relative bead position being influenced by neighbors up to 4 bead diameters away for $\epsilon = 0.355$ and up to 2 bead diameters away for $\epsilon = 0.71$. The distances over which the influence of one bead is felt would appear to confirm the idea that some kind of hydrodynamic interaction must be responsible, since only forces of this nature would be able to act over such large distances. A comparison between the lines for the two different values of ϵ shows that the surface separation between beads is much larger for the bigger gap. Wall effects are obviously important and one can imagine a situation where the gap is so large and the value of ϵ so small that no structuring is seen at all.

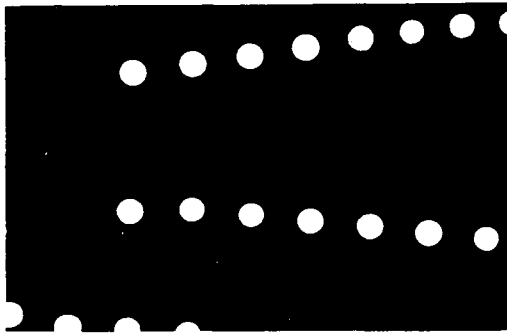
Figure 12 illustrates the results obtained using the 0.539 mm beads which, for the two different gaps used, give values for ϵ of 0.362 and 0.18. As can be seen the same general trends that were observed for the large beads occur once more. Again the bead separation decreases with an increase in shear rate and the larger gap width results in larger mean separations. Furthermore it has been found that by combining a wall



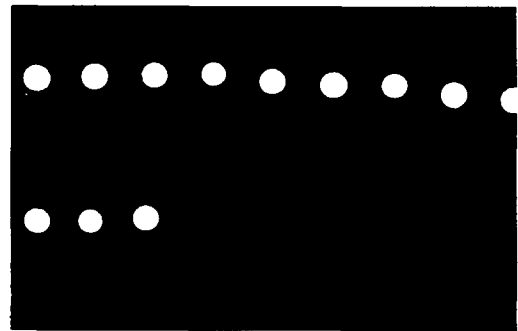
Shear Rate = 3.7 s^{-1} , $Re_p = 0.8$



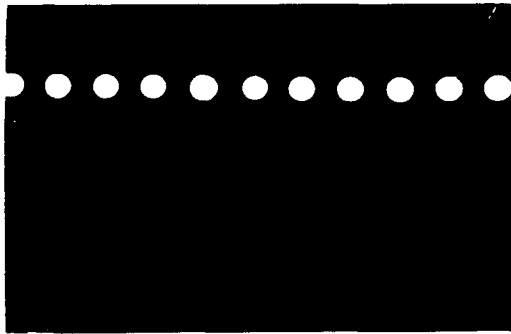
Shear Rate = 9.5 s^{-1} , $Re_p = 2.0$



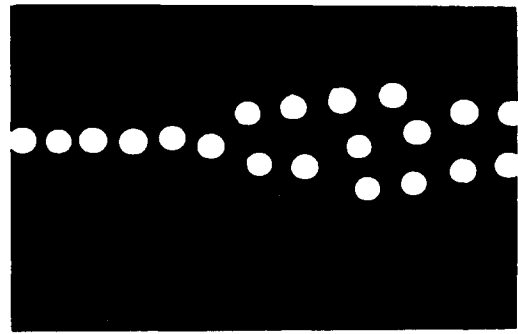
Shear Rate = 30 s^{-1} , $Re_p = 6.3$



Shear Rate = 45 s^{-1} , $Re_p = 9.4$



Shear Rate = 63 s^{-1} , $Re_p = 13.2$



Shear Rate = 123 s^{-1} , $Re_p = 25.7$

Figure 10. Series of photographs showing the effect of shear rate on the ordering phenomenon. Particle concentration = 27 beads/cm^3 , bead diameter = 1.059 mm , gap 1.5 mm , shear rate and Reynolds number given beneath each frame.

effect term with the particle Reynolds number, the data for all the values of ϵ studied collapse onto the same curve. This reduction is illustrated in Figure 13, where the reduced particle Reynolds number is simply the product of the particle Reynolds number and the appropriate value of ϵ . Plotting the same data on a logarithmic scale results in the straight line shown in Figure 14. It is therefore possible to write the following equation relating the separation between the beads to the reduced particle Reynolds number.

$$\log (\delta) = -0.41 \log (\text{Red.Re}) + 0.38 \quad \text{Regression coefficient} = 0.95$$

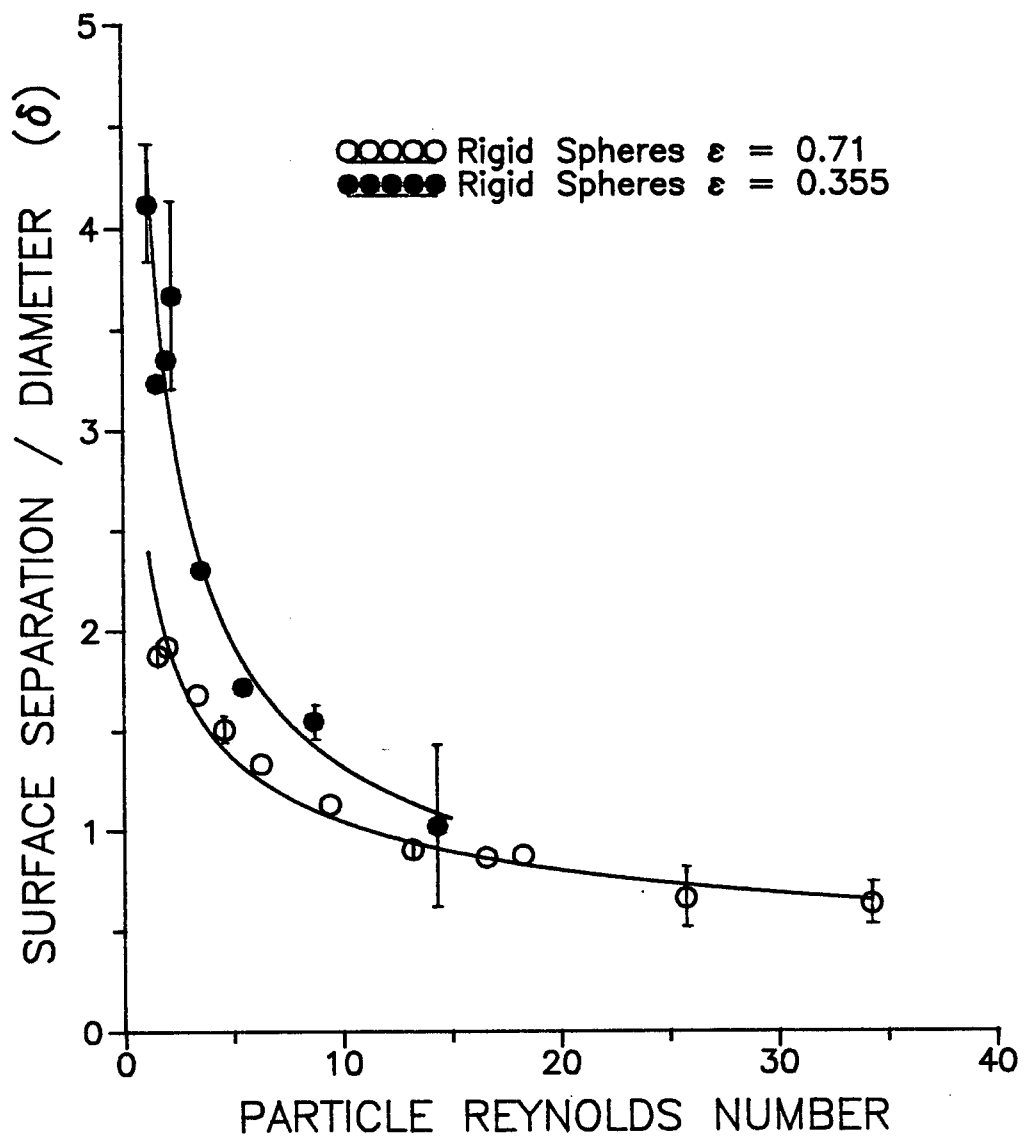


Figure 11. Surface separation/diameter ratio (δ) vs the particle Reynolds number for the larger beads.

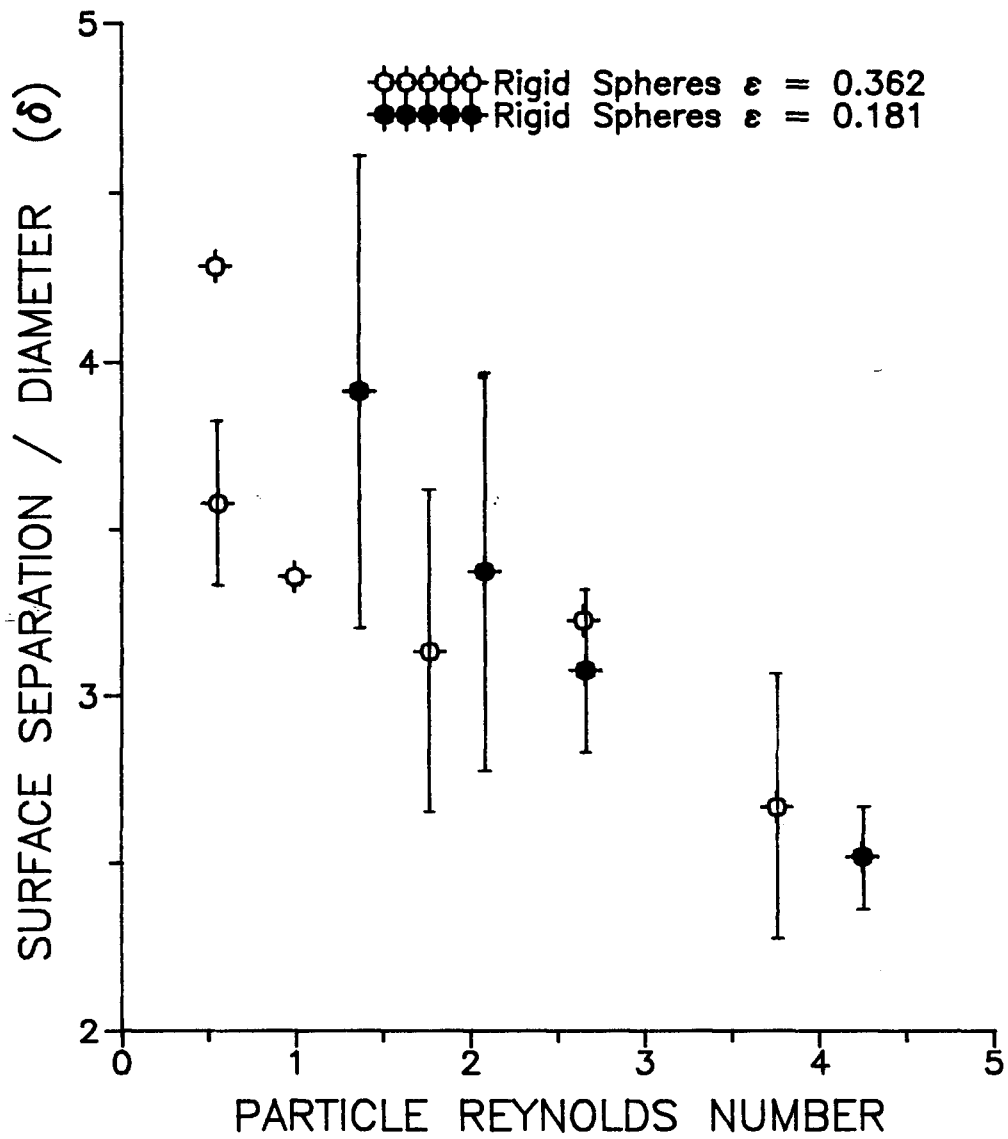


Figure 12. Surface separation/diameter ratio (δ) vs the particle Reynolds number for the smaller beads.

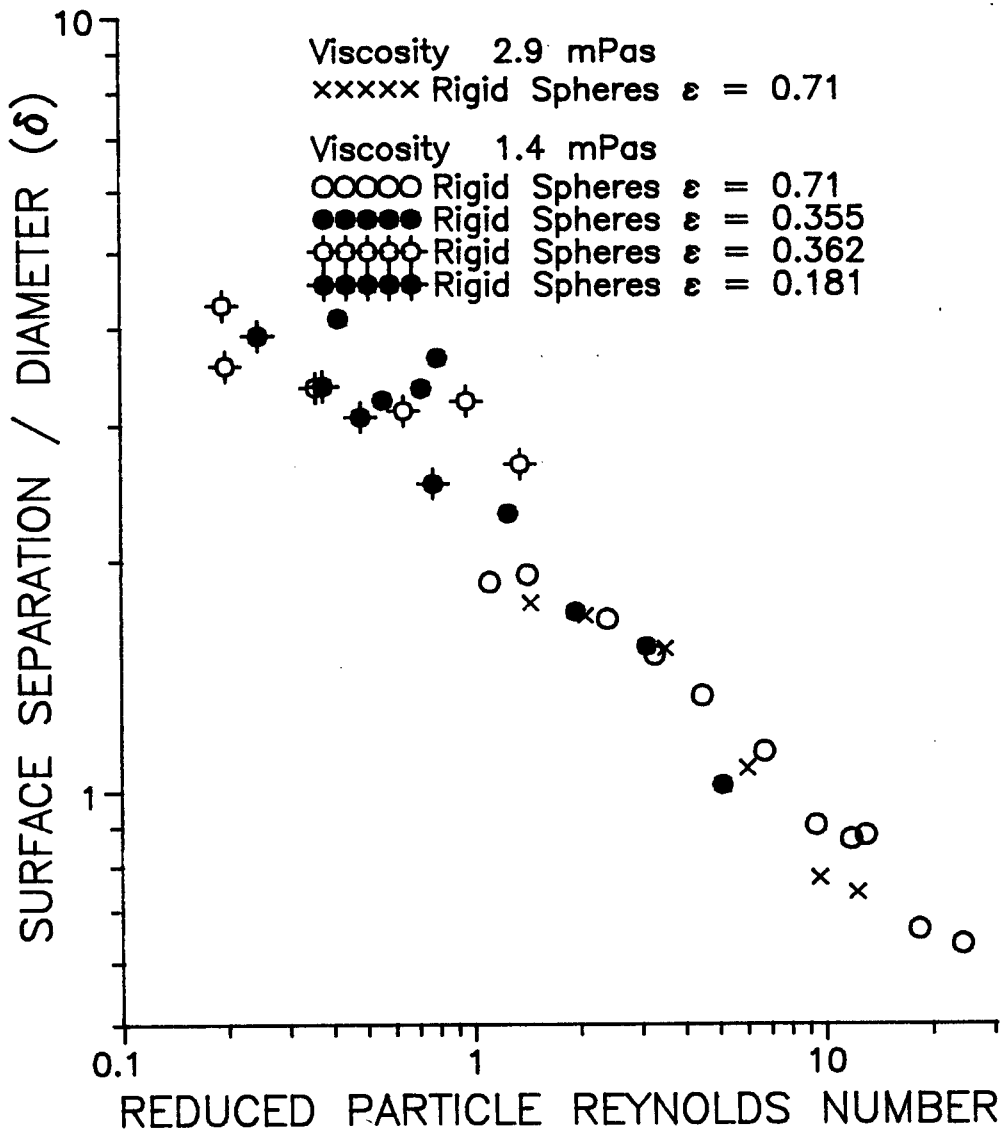


Figure 14. Logarithmic plot of surface separation/diameter ratio (δ) vs the reduced particle Reynolds number for several different values of ϵ .

3.4 Comparisons between rigid spheres and aggregated latex.

Since several variables appear to affect particle alignment, it seems prudent to make comparisons only between systems which have the particles rotating with roughly the same angular velocity and for which the values of ϵ are similar. This has been done in Table VIII which compares the particle separations between the rigid spheres and the aggregates in two different flow conditions. It is clear from this table

Table VIII

Comparison of the surface separations between
aggregated latex particles and rigid spheres

Conditions	ϵ	Re_p	Center Separation (mm \pm S.D)	Surface Separation (mm \pm S.D.)
0.05% Ltx.	0.71	2.71	2.2 \pm 0.1	1.1 \pm 0.2
1.44 M NaCl.	0.68	1.97	2.4 \pm 0.1	1.2 \pm 0.2

1.059 mm. beads in sucrose.	0.71	1.99	3.2 \pm 0.1	2.0 \pm 0.1

0.01% Ltx.	0.34	0.47	2.0 \pm 0.3	1.4 \pm 0.2
1.44 M NaCl	0.33	0.45	2.1 \pm 0.4	1.5 \pm 0.3

<u>(1.5 mm gap)</u>				
0.539 mm. beads in sucrose.	0.36	0.55	2.5 \pm 0.1	1.9 \pm 0.1
<u>(3.0 mm gap)</u>				
1.059 mm. beads in sucrose	0.36	1.15	5.5 \pm 0.3	4.4 \pm 0.3

that for similar values of Re_p and ϵ the separations between aggregated latex particles are in general smaller than those between rigid spheres.

Some insight into the processes responsible for the observed inter-particle separations can be gained by considering the flow around stationary particles of different shape and composition. One would expect the flow around the aggregates to be quite different from that around the rigid spheres, since, as well as being different shapes their internal structures are totally dissimilar. Interestingly, for the smaller aggregates whose shape is presumably closer to being spherical, the separations observed are closer to those seen with the rigid spheres. The volume of the wake behind ellipsoid particles is smaller than that behind a sphere (30), and surface roughness has the effect of delaying the separation of the boundary layer and decreasing the volume of the wake (31). Intuitively one would also expect the porous aggregates to have a much smaller disturbing effect on the fluid than the rigid spheres. These facts suggest that, for flow around stationary particles at least, the wake behind the aggregates would be smaller than that behind the rigid spheres. If this were also true for particles undergoing shear it might explain the observed differences in the inter-particle separations for the two types of particle. Indeed one could suggest that the distance of closest approach of the particles is limited by the size of the wake surrounding them.

Unfortunately this hypothesis is not supported by the observation that the inter-particle separation decreases as the Reynolds number increases. By analogy with flows around rigid spheres one would expect the wake to increase with increasing Reynolds number (30). Poe and Acrivos (32), however, observed that the stagnation points on either side

of a rigid sphere, rotating in simple shear flow, moved closer to the surface of the sphere as the Reynolds number increased. It could well be that the inter-particle separations scale with the distance of this stagnation point from the surface of the sphere.

These ideas do appear to provide a qualitative explanation for the differences in inter-particle separations observed. They do not, however, explain why or how the particles become aligned in the first place. Clearly there must be some force of attraction present between a particle and its neighbor. From the results presented in this thesis we know that this force must be able to act over distances of several particle diameters in the plane in which the shear forces are equal. One can therefore imagine a situation where this attractive force, which might for example result from the decreased pressure within the wake, pulls neighboring particles towards the surface of the particle. An opposing force must then keep the particles separated. Unfortunately, since no theoretical or experimental work has been reported for this particular flow regime, one is left to speculate as to the nature of these two opposing forces. Furthermore, as the work of Poe and Acrivos has yet to be repeated with a system of interacting spheres, it is not possible to test any hypothesis quantitatively.

CHAPTER FOUR

Conclusion

It has been shown that the particle alignment described in this thesis results from some type of hydrodynamic interaction which only occurs at particle Reynolds numbers sufficiently high to make inertial effects important. Comparisons between ordered aggregates and ordered rigid spheres rotating with similar angular velocities and similar diameter/gap ratios (i.e. wall effects approximately of the same magnitude) show that the surface separation for the aggregates is considerably smaller than the surface separation observed with the rigid spheres. It was pointed out that this difference reflects the size of the wake one would expect to see on either side of these aggregates. This led me to hypothesize that the surface separation between particles reflected the size of the wake between the particles. The decrease in surface separation observed with increase in particle Reynolds number was not, however, in agreement with this hypothesis. Poe and Acrivos (34), demonstrated that for single spheres rotating in a simple shear flow, the distance between the stagnation point and the surface of the sphere decreases with an increase in particle Reynolds number. It was suggested that the decrease in surface separation with increase in Reynolds number is somehow related to the movement of the stagnation point.

It is still unclear as to the nature of the hydrodynamic force which pulls particles separated by distances of many particle diameters into line, though one can speculate that such forces may result from a pressure drop at the front and back of the rotating particle. The nature of the wall effects are also uncertain but it has been clearly demonstrated in

this thesis that ordering will only occur when the aggregates reach sizes for which the influence of the wall must be considered.

Clearly before making any further speculations about the physical processes which result in this remarkable ordering phenomenon, some attempt must be made to model the system. This could be achieved numerically, using the appropriate equations and boundary conditions to calculate the nature of the streamlines around such interacting particles. Alternatively one could visualize the streamlines experimentally using tracer particles as Poe and Acrivos have already done for single spheres (32).

CHAPTER FIVE

Appendix

Table IX

The effect of shear rate on the aggregation kinetics

Gap width = 1.5 mm

Shear Rate (s^{-1})	1.8	3.7	7.3	9.4	11.3	15.8	18.7	21.4
Time for the appearance of first aggregates* (minutes).	9	10	7	5	5	5	3.5	3
Time for the appearance of first structure† (minutes).	17	15	9.5	7.5	7.5	7.5	5.5	5.5
Average aggregate diameter, 10 min. after structure observed (mm \pm S.D.)		0.72 \pm .11	0.67	0.74 \pm .11	0.78 \pm .1	0.66 \pm .11	0.66 \pm .11	0.54 \pm .09
Average surface separation, 10 min. after structure observed (mm \pm S.D.)		0.60 \pm .16	0.60 \pm .12	0.54 \pm .11	0.56 \pm .11	0.53 \pm .11	0.49 \pm .1	0.43 \pm .08

* "First aggregates" These were the first aggregates that could be visibly detected on the negative.

† "First Structure" Structure was defined as occurring when three or more aligned particles were observed.

Table X

Showing the effect of latex concentration on aggregation kinetics

Gap width = 1.5 mm

Latex Conc. (%w/w)	0.01	0.02	0.03	0.04	0.05	0.07	0.1	0.2
Time for the appearance of first structure* (minutes).	40	20	13	9	7		2	1
Time for the appearance of first structure† (minutes).	48	24	17	12	9.5		5	2
Average aggregate diameter, 10 min. after structure observed (mm ± S.D.)	0.34 ±.08	0.43 ±.11	0.49 ±.12	0.60 ±.11	0.67 ±.12	0.75 ±.11	0.75 ±.10	0.86 ±.05
Average surface separation, 10 min. after structure observed. (mm ± S.D.)	0.86 ±.23	0.79 ±.15	0.64 ±.10	0.61 ±.10	0.60 ±.16	0.62 ±.16	0.56 ±.13	0.62 ±.12

* "First aggregates" These were the first aggregates that could be detected visibly on the negative.

† "First Structure" Structure was defined as occurring when three or more aligned particles were observed.

Table XI

Growth of aggregates with time after mixing with NaCl

(NaCl = 1.44 M, shear rate = 21.4 s⁻¹,

latex Concentration = 0.05% w/w,

gap width = 1.5 mm)

Time After Mixing (minutes)	Mean Area ($\times 10^2 \text{ mm}^2$)	Standard Deviation ($\times 10^2 \text{ mm}^2$)
44	40.89	11.21
42	38.36	9.04
40	38.79	12.15
36	41.11	9.63
34	39.82	9.85
30	39.22	8.76
28	41.36	8.94
24	39.45	9.10
20	45.80	11.80
18	41.88	10.08
16	39.35	10.41
15	43.09	10.05
14	36.14	8.51
12	38.14	8.65
10	33.12	10.33
8	32.14	9.53
7	29.39	11.09
6	25.58	9.15
5	17.46	5.78
4	12.11	5.98
3	4.54	2.06

Table XII

Growth of aggregates with time after mixing with NaCl

(NaCl = 1.44 M, shear rate = 15.8 s⁻¹,

latex Concentration =0.05% w/w,

gap width = 1.5 mm)

Time After Mixing (minutes)	Mean Area ($\times 10^2 \text{ mm}^2$)	Standard Deviation ($\times 10^2 \text{ mm}^2$)
40	53.28	15.07
36	51.73	11.65
32	52.76	12.96
28	51.15	12.57
24	52.67	15.04
22	53.37	15.04
20	48.83	13.19
18	49.40	12.57
16	38.23	14.73
14	38.43	17.50
12	37.02	14.60
10	27.19	11.30
8	24.39	12.08
7	25.90	11.11
6	14.53	10.88
5	9.88	9.22
4	3.36	4.30

Table XIII

Growth of aggregates with time after mixing with NaCl
(NaCl = 1.44 M, shear rate = 11.28 s^{-1} ,
latex concentration = 0.05% w/w),
gap width = 1.5 mm)

Time After Mixing (minutes)	Mean Area ($\times 10^2 \text{ mm}^2$)	Standard Deviation ($\times 10^2 \text{ mm}^2$)
38	86.34	16.84
34	79.08	21.56
30.25	83.80	19.68
28	86.51	22.32
26	75.69	27.59
24	74.38	22.60
22	67.91	16.64
20	65.91	23.54
18	66.81	21.69
16	72.72	28.12
14	60.81	24.88
12	66.56	18.77
10	52.31	17.82
8	49.71	17.51
7	44.95	19.32
6	32.29	16.93
5	26.85	14.58
4	9.18	6.70
3	6.69	6.68

Table XIV

Growth of aggregates with time after mixing with NaCl

(NaCl = 1.44 M, shear rate = 5.55 s^{-1} ,

latex concentration = 0.05% w/w),

gap width = 1.5 mm)

Time After Mixing (minutes)	Mean Area ($\times 10^2 \text{ mm}^2$)	Standard Deviation ($\times 10^2 \text{ mm}^2$)
60.75	62.60	32.30
44.75	68.44	28.34
39.9	95.34	27.45
36	78.55	25.81
32	82.83	30.43
30	81.06	30.82
28	70.95	20.92
26	94.09	41.64
24	72.08	25.94
22	81.68	31.74
20	65.34	32.37
18	57.96	33.61
16	46.32	24.38
14	51.92	32.43
12	43.50	20.62
10	38.32	29.48
9	15.79	12.39

References

1. J.W. Goodwin, Some Uses Of Rheology In Colloid Science. In: Colloidal Dispersions, J.W. Ed., The Royal Society of Chemistry, London(1982). p. 165.
2. Th. F. Tadros, Adv. Colloid Interface Sci., **12** 141 (1980).
3. R. Buscal, J.W. Goodwin, M.W. Hawkins and R.H. Ottewill, J.Chem.Soc. Faraday I, **78** 2873 (1982).
4. Th. F. Tadros, Chemistry and Industry, April 1985, p.210.
5. H. Van Olphen, Clay Minerals, **4** 68 (1956).
6. T.G.M van de Ven and S.G. Mason, J. Colloid Interface Sci., **57** 505 (1976).
7. T.G.M. van de Ven and S.G. Mason, J. Colloid Interface Sci., **57** 535 (1977).
8. T.G.M. van de Ven and S.G. Mason, Colloid Polym. Sci., **255** 794 (1977).
9. W.R. Schowalter, Ann. Rev. Fluid Mech., **16** 245 (1984).
10. R.M. Fitch, Polymer Colloids Plenum, New York, (1971).
11. P.A. Hiltner and I.M. Krieger, J. Phys. Chem., **73** 2386 (1969).
12. L. Barclay, A.H. Harrington and R.H. Otterwill, Kolloid Z.Z. Polym., **250** 655 (1972).
13. A. Kose, M. Ozaki, K. Takano, Y. Kobayashi and S. Hachisu, J. Coll. Int. Sci., **44** 330 (1973).
14. R. Williams and R.S. Crandall, Phys. Lett., **48A** 225 (1974).
15. R.L. Hoffman, Trans. Soc. Rheol, **16** 155 (1972).
16. B.J. Ackerson and N.A. Clark, Physica, **118A** 221 (1983).

17. A.D. Olal, A Surface And Colloid Chemical Study Of The Interaction Of Proteins With Polystyrene Latex. PhD. Thesis, U.B.C. 1990.
18. B.V. Derjaguin, L. Landau, Acta Physiochim., **14** 633 (1941).
19. E.J. Verwey, J.Th.G. Overbeek, Theory Of The Stability Of Lyophobic Colloids. (1948) Elsevier, Amsterdam.
20. D.H. Everett, The Basic Principles Of Colloid Science. (1988) The Royal Society of Chemistry Paperbacks, London.
21. R.G. Cox, I.Y.Z. Zia, and S.G. Mason, J. Colloid Interface Sci., **27** 7 (1968).
22. P.A. Arp, and S.G. Mason, J. Colloid Interface Sci., **61** 21 (1977).
23. P.M. Adler, J. Colloid Interface Sci., **84** 461 (1981).
24. T.G.M. van de Ven, Colloidal Hydrodynamics, chapter 5, (1989) Academic Press.
25. T.G.M. van de Ven, PhysicoChem. Hydrodynam., **10** 97 (1988).
26. S. Wakiya, C.L. Darabaner, and S.G. Mason, Rheol. Acta., **6** 264 (1967).
27. H.L. Goldsmith and S.G. Mason, The Microrheology Of Dispersions. In: Rheology, Theory And Applications, F. Eirich Ed., Academic Press, New York, (1976). p.85.
28. R.H. Weiland, Y.P. Fessas and B.V. Ramarao, J. Fluid Mech., **142** 383 (1984).
29. S.C.R. Dennis and J.D.A. Walker, J.Fluid Mech., **48** 771 (1971).
30. R. Clift, J.R. Grace and M.E. Webber, Bubbles, Drops, And Particles. Academic Press, (1978).
31. P.M. Gerhart and R.J. Gross, Fundamentals Of Fluid Mechanics, Addison-Wesley Publishing Company (1985) chapter 8.
32. G.G. Poe and A. Acrivos, J. Fluid Mech., **72** 605 (1975).

33. G. Segré and A. Silberberg, J. Fluid Mech., **14** 115 (1962).
34. G. Segré and A. Silberberg, J. Fluid Mech., **14** 136 (1962).
35. B.P. Ho and L.G. Leal, J. Fluid Mech., **65** 365 (1974).
36. G. Segré, 1963 Proc. 4th Int. Congr. Rheol., pt. 4.
37. K. Bauckhage, Biorheology, **12** 329 (1975).
38. D.J. Shaw, Introduction To Colloid And Surface Science, 2nd Edition, p 191, Butterworths 1970.
39. R.B. Bird, W.E. Stewart and E.N. Lightfoot, Transport Phenomena, p. 95. John Wiley and Sons, Inc. 1960.